A Micro-Macro Approach to Predict Stiction due to Surface Contact in Micro Electro- Mechanical Systems

Ling WU, Ludovic NOELS, Véronique ROCHUS, Marius PUSTAN, Jean-Claude GOLINVAL

***Abstract*—Stiction, which results from contact between surfaces, is a major failure mode in micro electro-mechanical systems (MEMS). Indeed microscopic structures tend to adhere to each other when their surfaces enter into contact and when the restoring forces are unable to overcome the interfacial forces. Since incidental contacts cannot be completely excluded and since contacts between moving parts can be part of the normal operation of some types of MEMS, stiction prediction is an important consideration when designing micro and nano-devices. In this paper a micro-macro multi-scale approach is developed in order to predict possible stiction. At the lower scale, the unloading adhesive contact-distance curves of two interacting rough surfaces are established based on a previously presented model [L. Wu et al., J. Appl. Phys. 106, 113502, 2009]. In this model, dry conditions are assumed and only the van der Waals forces as adhesion source are accounted for. The resulting unloading adhesive contact-distance curves are dependant on the material and on surface properties, such as, elastic modulus, surface energy and on the rough surfaces topography parameters; the standard deviation of asperity heights and the asperities density. At the higher scale, a finite element analysis is considered to determine the residual cantilever beam configuration due to the adhesive forces once contact happened. Toward this end, the adhesive contact-distance curve computed previously is integrated on the surface of the finite elements as a contact law. Effects of design parameters can then be studied for given material and surface properties.**

Index Terms—Stiction, Micro-electro-mechanical system, Contact, Rough surfaces, Multi-scale

Manuscript received August 12, 2010. This work was supported by the project COROMIS, "First Postdoc Project 2007" funded by the Walloon Region of Belgium and the Belgian National Fund for Scientific Research.

L. Wu is with the Aerospace and Mechanical Engineering Department, University of Liege, 1 Chemin des Chevreuils, B52, 4000 Liège Belgium, and with the Northwestern Polytechnical University, 710072 Xi'an China (phone: +32-4-366-9453; fax: +32-4-366-9217; e-mail: L.Wu@ulg.ac.be).

L. Noels is with the Aerospace and Mechanical Engineering Department, University of Liege, 1 Chemin des Chevreuils, B52, 4000 Liège Belgium (e-mail: L.Noels@ulg.ac.be).

V. Rochus was with the Aerospace and Mechanical Engineering Department, University of Liege, Belgium and is now with IMEC, Kapeldreef 75, 3001 Leuven (e-mail: Veronique.Rochus@imec.be)

M. Pustan was with the Department of Machine Elements and Tribology, Technical University of Cluj-Napoca, Romania. He is now with the Aerospace and Mechanical Engineering Department, University of Liege, 1 Chemin des Chevreuils, B52, 4000 Liège Belgium (e-mail: M.Pustan@ulg.ac.be).

J. C. Golinval is with the Aerospace and Mechanical Engineering Department, University of Liege, 1 Chemin des Chevreuils, B52, 4000 Liège Belgium (e-mail: JC.Golinval@ulg.ac.be).

I. Introduction

RECENTLY, micro electro-mechanical systems (MEMS) have drawn attention due to their miniature sizes, low power requirements and reduced manufacturing costs. In industry [1], several applications, such as accelerometers, digital mirror devices, pressure sensors, gyroscopes or resonators have been realized using MEMS technologies and many new applications are under development. In spite of those advantages, the inherent characters of MEMS, such as, the large surface-area to volume ratio, the relatively smoothness of the surfaces, the small interfacial gaps and the small restoring forces make them particularly vulnerable to the surface forces that could lead to permanent adhesion of MEMS moving parts. This stiction phenomenon can severely affect the reliability of these devices.

The term 'stiction' is a combination of stick and friction and is now used to refer to any kind of adhesion that can occur between micro components. There are mainly two kinds of stiction in MEMS [1, 2], the 'release stiction' and the 'in-use stiction'. Release stiction refers to the kind of stiction happening during the fabrication process at etching of the final sacrificial layer, in which the suspended structures may adhere to the substrate due to the tremendous capillary forces and to the relatively low restoring force of the structures. In-use stiction occurs during the normal operation of MEMS devices when two surfaces enter into contact and permanently adhere to each other. This kind of failure typically happens for devices involving on-and-off contact of surfaces such as scratch drive actuators or RF switches, but also for devices for which surfaces always work in contact, such as gears.

Although release stiction can be avoided by using hydrophobic coating and in-use stiction risk can be reduced by operating the devices in dry or vacuum environment, where the capillary forces can be reduced to the negligible level [3, 4], in-use stiction cannot be completely eliminated due to the existence of the van der Waals forces.

Therefore numerical models are required in order to make this kind of failure predictable and avoidable. In order to predict this failure mode, a micro-macro multi-scale model is developed in this paper; at the lower scale the adhesive contact forces of two rough surfaces are predicted, and at the higher scale a finite element analysis is considered, in which the

adhesive contact-distance curve computed at the lower scale is integrated on the surface of the finite elements as a contact law.

In order to model the adhesive contact forces it has been revealed that in the dry environment, where the capillary forces can be neglected, the surface energies and the related surface forces (e.g. van der Waals (VDW) forces) are the key factors to be considered [1, 4]. It has been shown in [4] that below 30% of relative humidity the force due to capillary condensation is reduced and that the adhesion is dominated by the molecular van der Waals forces. However, as discussed in [4], and as it will be discussed in details in section III.A, the operating medium and the surface treatment will have effects on the van der Waals adhesion effect, unless experiments are performed in ultra-high vacuum and surfaces are previously cleaned.

In the presence of van der Waals forces, two earlier theories of adhesive contact between an elastic sphere and a flat surface have been developed, the Johnson-Kendall-Roberts (JKR) model [5] and the Derjaguin-Muller-Toporov (DMT) model [6]. The JKR model is ideal for soft materials with a large contact curvature surface and a high surface energy. The DMT theory, in contrast, is well suited for hard materials with a reduced contact curvature and a low surface energy. This apparent contradiction between the JKR model and the DMT model is solved by considering a dimensionless parameter, μ_T (Tabor number), introduced by Tabor [7]. This parameter is used to characterize the ratio between the elastic deformations at pull-out and the interaction range of the surface forces. For the JKR model to be valid, μ_T should be larger than 5, while for the DMT model, μ_T should be lower than 0.1. Subsequently, Maugis, [8], provided a transition solution for intermediate cases between JKR and DMT regimes. In this model the transition between the two regimes is characterized by the Maugis transition parameter, λ, which involves surface and material properties. For completeness, note that the adhesive contact between a sphere and a flat surface has also been studied by numerical analyses [9, 10], where some solutions were given using curve fitting of the numerical results.

Maugis theory, [8], is an analytical theory based on the Dugdale assumption of inter-atomic attractions. Within a critical distance two surfaces are attracted with a constant force per unit area. If the separation exceeds this threshold the adhesive traction immediately falls to zero. The induced discontinuity resulting from this model can lead to inaccuracies, [11], especially in the case of soft materials [12], for which the Maugis model is unable to predict pre-contact deformations. The use of a Lennard-Jones (LJ) potential, substituting the Dugdale assumption for the adhesive part in combination to the Hertz theory shows the apparition of hysteretic curves during transitions from no-contact to contact conditions (jump-into-contact) and from contact to no-contact conditions (jump-out-of-contact), [12-17]. In particular, a jump-in induced yield criterion was developed in [16] based on semi-analytical results. This criterion was exploited in [17] for cyclic loadings. Finally, the LJ models can be combined with FE methods to study elasto-plastic behaviors during contact, see [18] among others.

These former theories are dealing with the problem of the single asperity contact. Owing to the roughness property of real micro surfaces, study of the adhesion problems based on rough surfaces is mandatory for MEMS. There are mainly two approaches used to characterize the surface topography and that have been considered in contact mechanics. The first one is the statistical approach introduced by Greenwood and Williamson (GW) [19] for which the rough surfaces are simulated by multi-asperities with random height distribution [20]. As an extension to the single asperity contact theories mentioned previously, this GW asperity model is widely used to study the adhesive contact between two rough micro-surfaces [21, 22]. The second approach, based on fractal geometry [23], captures the multi-scale nature of the surface topography and has been considered by Majumdar and Bhushan [24] to develop a fractal-based description of surfaces contacts.

However, these theoretical studies are cumbersome when applied directly to predict the stiction in complete MEMS structures due to the difficulty of measuring the distance between asperities of two interacting surfaces. In order to overcome this difficulty several studies have been conducted for modeling stiction in MEMS by considering the so-called apparent adhesion energy. Tas et al. [25] investigated the different mechanisms that contribute to the adhesion forces, and considered the effects of the entire adhesive sources in this apparent adhesion energy. Based on the energy equilibrium of deformed structures they gave the critical length leading to in-use stiction of cantilever and double clamped beam structures. Boer et al. [26, 27], quantified the apparent adhesion energy on micro cantilever beams by measuring the deflected shapes of the beams and by reproducing them with the finite element method. In these approaches all effects, such as environment, roughness of surfaces and material properties are included in the apparent adhesion energy.

The finite element method was also applied by Lie et al. [28], to analyze the effect of adhesive contact on MEMS switches. They assumed a constant adhesive force between the contacting surfaces, which is not always rigorous and has less physical basis. For completeness, another approach is to consider finite element simulations of a reduced number of interacting asperities combined with capillary and van der Waals forces interactions, [29].

It appears that in order to consider a proper model of adhesive forces for rough surfaces interactions when designing a deformable or moving MEMS, a multi-scale approach should be developed. In this study the higher scale is constituted by a finite element analysis of the structures entering into contact. The lower scale corresponds to the adhesion/contact model previously developed in [22] (based on Maugis and Kim formulations). This adhesion/contact model can directly be integrated on the surfaces of the finite-elements. In this work, the use of the Maugis-Kim formulations instead of a more complex LJ-based solution is justified as interest lies only in the unloading curves when predicting stiction. The paper also focuses on relatively hard materials, as polysilicon, which do not exhibit elasto-plastic behavior during contact interactions.

This multi-scale model is applied to a clamped/free beam as an illustration. Clamped/free beams are usually considered to study stiction effect, [26]. Main interest in considering such cantilever beams in this work is the possibility to extract the apparent adhesion energy from the numerical simulations and thus to discuss and compare our micro-macro model with literature. In particular it is shown that the approach allows considering different design parameters for given surface and material properties.

The layout of the paper is as follows. In section II the theory of the statistical adhesive contact model for rough surfaces developed in [22] is reviewed. For different Maugis transition parameters and for different standard deviations of asperity heights the curves of the adhesive-contact forces against distances of two rough surfaces are presented as demonstrations. In section III, these curves are presented for the case of interactions between polysilicon surfaces. In particular three samples of polysilicon equivalent surfaces obtained from atomic force microscopy (AFM) measurements are retrieved from the literature and analyzed. Therefore, the adhesive contact model described in section II can be applied to obtain the relationship between the contact force and the surfaces' distance. Based on the knowledge of these forces, the residual configurations of micro clamped/free beams are analyzed using the finite element method. This multi-scale approach is described in section IV for a Timoshenko finite element model of a beam. The adhesion contact force curves obtained in section II are then integrated on the beam surface interacting with a planar part (e.g. landing pad). In section V, the adhesion contact force curves obtained in section III for polysilicon-to-polysilicon interactions are used in the multi-scale model in order to predict the design parameter's range of the micro-cantilevers for different surface topographies. As way of an example, for different surface gaps, the critical height to length ratio of the beam leading to stiction is provided. The presented model is compared, in section VI, to literature models and in particular the apparent adhesion energy, [26-27], is extracted to validate the presented method.

II. The Adhesive Contact between Two Rough Surfaces

In this section, the adhesive contact theory developed in our previous work [22] is briefly reviewed. This model is based on the combination of Greenwood-Williamson model and Maugis transition's theory. This developed framework is then exploited to derive adhesive contact vs. distance curves for different material and surface properties.

A. Greenwood–Williamson Model and Adhesive Contact Theory

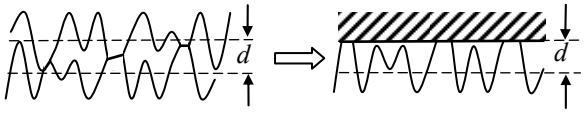

Fig. 1. Contact of two rough surfaces and the equivalent rough surface at a separation distance *d*.

Based on the research of Greenwood and O'Callaghan [20, 30], the contact of two rough surfaces can be represented by the contact between an equivalent rough surface and a smooth plane, with negligible difference (Fig. 1).

In Greenwood and Williamson 'asperity-based model' [19], the rough surface is described by a collection of spherical asperities with identical end radii, whose heights h have a statistical distribution. For two initial contacting rough surfaces with asperity end radii R_1 and R_2 respectively, and standard deviations in asperity heights σ_1 and σ_2, the equivalent rough surface is defined by the asperities end radius $R=R_1R_2/(R_1+R_2)$ and the standard deviation in asperity heights by $\sigma_s=(\sigma_1^2+\sigma_2^2)^{1/2}$. Usually [19], a Gaussian distribution is used to describe the asperity heights distribution of the equivalent rough surface:

$$\varphi(h)=\frac{1}{\sigma_s\sqrt{2\pi}}\exp(\frac{-h^2}{2\sigma_s^2}) \quad (1)$$

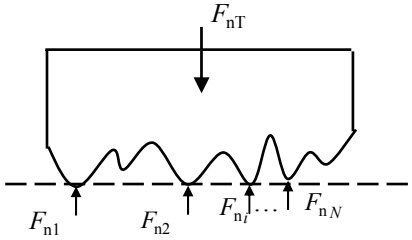

Fig. 2. Schematic view of the contact forces between the equivalent rough surface and the smooth plane represented by the dashed line.

The Gaussian distribution (1) characterizes the probability density function along the vertical axis (height). Another function should be defined to represent the spatial horizontal correlation of ordinates. A widely used function, under the assumptions of stationary and ergodicity of the surface, is the exponential autocorrelation function (ACF), [1]. The ACF allows the determination of a characteristic length related to the spatial occurrence of given surface heights and thus, of the number of interacting asperities. In the present work the spatial horizontal distribution is represented by the asperity density, N, and the asperity tip radius R as required by Maugis theory [8]. These values, as well as the ACF, can be deduced from AFM measurements, as explained in section III.B.

The contact force between the equivalent rough surface and a smooth plane can be obtained as a function of the surfaces distance defined as the separation between the two rough surfaces mean planes of asperity heights. When considering the equivalent rough surface, this distance, d, is defined as the distance from the equivalent rough surface mean plane of asperity heights to the smooth surface (Fig. 1). The total contact force F_{nT} can be expressed as the sum of the contact forces F_{ni} (i=1,2,…N) on each asperity (see Fig. 2), with

$$F_{nT}=\sum_{i=1}^{N}F_{ni} \quad (2)$$

The contact forces F_{ni}, which include the Hertz contact forces due to the elastic deformations of the asperities at micro contacts and the adhesion forces due to van der Waals attractive

forces, can be calculated using the Maugis adhesive contact theory combined with Kim expansion [8, 31], as it has been developed in [22].

Maugis theory [8] is an analytical model based on the Dugdale assumption of inter-atomic attractions. Within a critical value of separation z_0, two surfaces are attracted with a constant force per unit area, σ_0. If the separation, z, exceeds this threshold z_0, the adhesive traction immediately falls to zero. In order to characterize the importance of the adhesive traction with respect to the Hertz elastic deformation pressure, Maugis transition parameter is defined as

$$\lambda = \frac{2\sigma_0}{(\pi\varpi K^2/R)^{1/3}} \tag{3}$$

where R is the effective radius of the equivalent rough surface and K is the reduced elastic modulus. This reduced elastic modulus is defined as $K=4/3\cdot[(1-\nu_1^2)/E_1+(1-\nu_2^2)/E_2]^{-1}$, where E_1, E_2, ν_1 and ν_2 represent the Young's modulus and Poisson's ratio of the respective materials the two interacting bodies are made of. The adhesive energy ϖ is given by $\varpi = \gamma_1 + \gamma_2 - \gamma_{12}$, where γ_1 and γ_2 represent the surface energies of each interacting body and γ_{12} is the interface energy of the two materials. Under the Dugdale assumption the adhesive energy satisfies the relation $\varpi = \sigma_0 z_0$. The value of λ defined by Eq. (3), ranges from zero to infinity, with the limiting case of compliant materials with large asperity tips radius and high adhesive energy leading to $\lambda=\infty$. For the limiting case of rigid materials with small asperity tips radius and low surface adhesive energy $\lambda=0$.

The three governing equations of Maugis theory [8] for the transition solution of two adhesive spheres in contact are

$$1 = \frac{\lambda A^2}{2}[\sqrt{m^2-1} + (m^2-2)\arctan\sqrt{m^2-1}] + \frac{4\lambda^2 A}{3}[\sqrt{m^2-1}\arctan\sqrt{m^2-1} - m + 1] \tag{4}$$

$$\overline{F}_n = A^3 - \lambda A^2(\sqrt{m^2-1} + m^2\arctan\sqrt{m^2-1}) \tag{5}$$

$$\Delta = A^2 - \frac{4}{3}A\lambda\sqrt{m^2-1} \tag{6}$$

where the parameter m is equal to c/a, c being the adhesive interaction radius (i.e. the part of the asperity subjected to adhesive forces) and a being the intimate contact radius (i.e. the part of the asperity subjected to Hertz contact forces), see Fig. 3(a). A, $\overline{F}_n$ and Δ are the dimensionless contact radius, load (positive if compressive) and approach (interference) respectively. They are defined as follows;

$$A = \frac{a}{(\pi\varpi R^2/K)^{1/3}} \tag{7}$$

$$\overline{F}_n = \frac{F_n}{\pi\varpi R} \tag{8}$$

$$\Delta = \frac{\delta}{(\pi^2\varpi^2 R/K^2)^{1/3}} \tag{9}$$

where the approach (interference) δ is found to be

$$\delta = \frac{a^2}{R} - \frac{8\sigma_0}{3K}\sqrt{c^2-a^2} \tag{10}$$

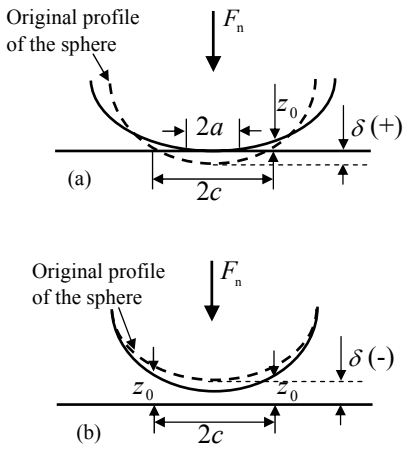

Fig. 3. Illustration of the physical parameters. (a) Contact radius a and adhesive contact radius c, the interference δ is a positive value for original Maugis theory. (b) In Kim et al. extension, interference δ is a negative value.

Kim et al., [31], extended the Maugis-Dugdale solution to the non-contact regime of $a = 0$ and $c \neq 0$ (see Fig. 3(b)) by the adjustment of Maugis governing equations (4-6), see [22] for details. Practically this extension has to be considered when $\lambda<0.938$. As a general case, the determinations of the contact force (8), interference (9) and contact radius (7) can be solved with Maugis theory and Kim extension, and, as a result, for a given value of λ, the dimensionless contact force $\overline{F}_n$ is obtained as a function of the dimensionless approach, Δ (interference).

From the definition of the distance, d, the approach (interference) δ, of an asperity of height, h, is equal to h-d and using similar normalizations as for Eqs. (8) and (9), the contact force per unit area, (2), between the two rough surfaces can be rewritten in the dimensionless way as

$$\overline{F}_{nT} = \sum_{i=1}^{N}\overline{F}_{ni} = N\int_{-\infty}^{\infty}\overline{F}_n(\overline{h}-\overline{d})\varphi(\overline{h})d\overline{h} \tag{11}$$

where the density of asperities N is the number of asperities per unit surface area. However, as some asperities located further than a critical approach Δ_1 are not subjected to adhesive-contact forces, the integration interval of Eq. (11) can be reduced. It should be noted that due to adhesion during the unloading process, asperities may remain in contact even if the initial height of asperities is lower than the equilibrium separation. Moreover, due to these adhesive forces the deformed position may be maintained within the distance z_0 in which the adhesive forces are still acting. Therefore, the lower limit of integration Δ_1 has a negative value in order to take into account this adhesion effect. For $\lambda \geq 0.938$, Δ_1 corresponds to the abrupt pull-out approach Δ_C, defined by Kim extension theory, and for $\lambda < 0.938$, Δ_1 equals $-2/(\pi\lambda)$ [22].

Removing the part of asperities on which contact forces are zero and using the asperity heights distribution of the equivalent rough surface (1), Eq. (11) can be written in terms of the dimensionless approach (interference) Δ

$$\overline{F}_{\mathrm{nT}}(\overline{d}) = \frac{N}{\overline{\sigma}_s\sqrt{2\pi}}\int_{\Delta_1}^{\infty}\overline{F}_{\mathrm{n}}(\Delta)\exp(-\frac{(\Delta+\overline{d})^2}{2\overline{\sigma}_s^2})d\Delta \qquad (12)$$

where $\overline{\sigma}_s$ equals the standard deviation of asperity heights σ_{s} divided by $(\pi^2\varpi^2R/K^2)^{1/3}$.

It should be noted that Eq. (12) is valid only during the unloading part following a contact configuration.

B. Analysis of Results and Discussion

From Eq. (12), it can be found that the dimensionless contact force, $\overline{F}_{\mathrm{n}}$, per unit area at a certain contact distance, *d,* depends on the Maugis transition parameter, λ, and on the rough surface topography parameters: the density of asperities, *N,* and the standard deviation of asperity heights, σ_{s}. In this section, Eq. (12) is applied in order to analyze the relation between the adhesive contact force and the contact distance during the unloading process. As a way of illustrating this process, Maugis transition parameter of the equivalent rough surface is successively set to be 0.1, 0.5 and 1.0. Fig. 4 (a)-(c) show the contact force vs. contact distance curves (described by Eq. (12)) for these three values of λ and for standard deviations of asperity heights, σ_{s}, equal to 0.5, 0.6, 0.7 and 1.0 nm respectively.

In Fig.4, the contact force is presented in a dimensionless way with $F_{\mathrm{nT}}/(N\pi\varpi R)$ (which equals $\overline{F}_{\mathrm{n}}/N$) and the distance is represented by d/σ_{s}. Positive forces represent compression and negative forces represent adhesion between the two interacting surfaces. In the curves it clearly appears that when the surfaces are in contact Hertz forces lead to a resulting positive compressive force. When the distance increases, the contact compressive forces are progressively released, but as adhesive forces are still acting, the resulting force becomes negative at a given distance. This corresponds to surface attraction. Finally if the distance keeps increasing, the adhesion forces are decreasing and the resulting force tends toward zero.

From Fig. 4(a-c) it can be observed that the lower the value of λ of the equivalent rough surface, the lower the amplitude of the adhesive force. This was expected as a low value of λ corresponds to a low work of adhesion, ϖ, of the surfaces. Another result is that when λ decreases, the maximum adhesive force (in module) is reached for higher non-dimensional distances and the compressive forces are more important at low distance. This means that the asperities on rough surfaces with high λ are easier to be deformed than asperities of rough surfaces with low λ. The effect of the standard deviation of asperity heights, σ_{s}, is similar for the different values of λ; adhesive forces between the surfaces decrease with the increase of σ_{s}, as the number of asperities interacting rapidly decreases.

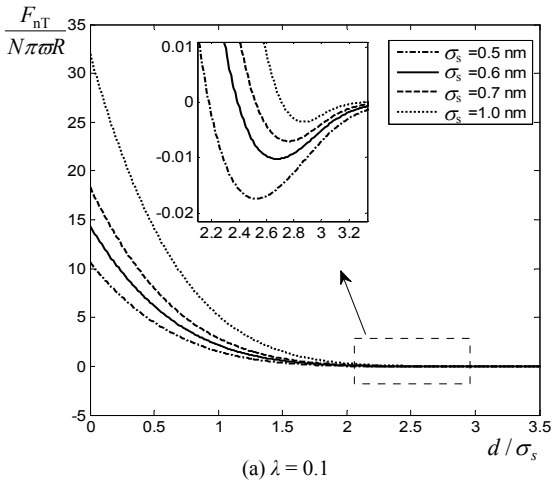

(a) λ = 0.1

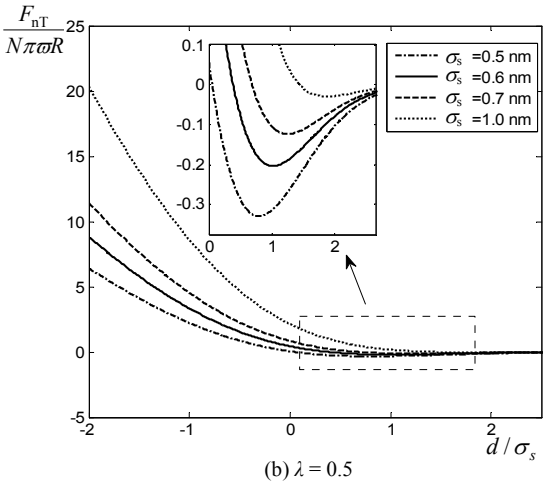

(b) λ = 0.5

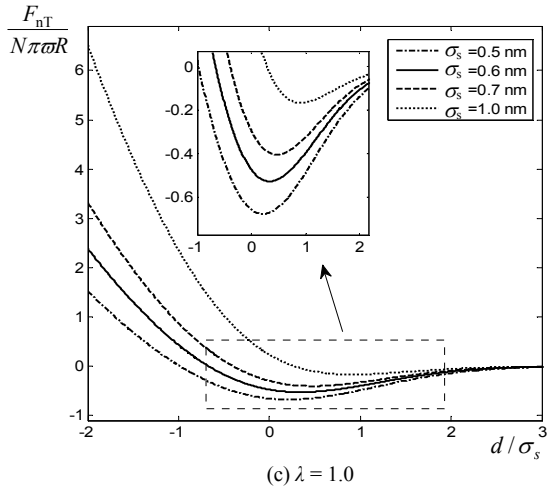

(c) λ = 1.0

Fig. 4. The normalized adhesive contact force vs. the normalized distance between the rough surfaces for different λ.

All the curves presented in Fig. 4 correspond to unloading contact - distance curves. As generating these curves for a given set of parameters is time consuming, they are fitted with polynomial approximations before being used in finite element simulations.

III. Polysilicon to Polysilicon Interaction

Polysilicon, which consists into an aggregate of mono-crystalline silicon grains, is widely used in MEMS due to the well-mastered deposition manufacturing process and to its excellent material properties (high Young modulus, good rupture resistance, low thermal expansion coefficient, etc)[34].

However, especially for polished surfaces, polysilicon to polysilicon interactions happening in MEMS devices can lead to stiction. This justifies its study in the present paper. Non-exhaustive typical applications are the support-spring of comb-drive actuators [25] (in which stiction between comb teeth could be induced by mechanical shocks) or the micro-machined flaps [35] (in which stiction could occur between the movable plates and substrate).

Moreover, depending on the surface state, interaction between asperities can remain mainly elastic, as it will be shown later on, which fits the use of our Maugis-based model.

In order to generate the curves presented in section II for this particular case, the material and surface properties have to be determined.

A. Adhesive Parameters

According to the descriptions of Maugis theory and Dugdale assumption, the adhesive energy per unit area, ϖ, is the energy per unit area required to separate two bodies (1 and 2), of perfectly flat surfaces, in contact. Based on the Lennard-Jones potential, the expression of adhesive energy is deduced from the work expended to move the two half-spaces from the equilibrium distance D_0, to infinity [8, 33], leading to

$$\varpi = \frac{A}{16\pi D_0^2} \tag{13}$$

where $A = 4\varepsilon\pi^2\rho_1\rho_2 r_0^6$ is the Hamaker constant, ε is the potential energy between two atoms at equilibrium distance, r_0 is the (finite) distance at which the inter-particle potential is zero, and where ρ_1 and ρ_2 are the numbers of atoms per unit volume of the two bodies respectively. In the case of pure silicon to pure silicon interactions, these parameters can be found in the literature: $\varepsilon = 3.47 \times 10^{-19}$ J [36], $r_0 = 2.09$ Å [33, 36], and $\rho_1 = \rho_2 = 4.975 \times 10^{28}$ /m^3, leading to a Hamaker constant of $A = 2.83 \times 10^{-18}$ J. The equilibrium distance D_0, at which the force between two half-spaces is zero, is given by $D_0 = (2/15)^{1/6} r_0$ [33], leading to $D_0 = 1.49$ Å. Using these values the adhesive energy (13) can be computed as ϖ 2.54 J/m^2.

The adhesive energy can also be calculated from the surface energy γ. If two bodies in contact are made of the same material, the adhesive energy is twice the surface energy γ of the material. Theoretically, for crystals, this energy can be estimated by considering cleavage in the lattice. It will depend on the lattice structure but also on the cleavage plane orientation. An experimental result of surface energy $\gamma = 1.24$ J/m^2 is given in [37] for silicon. This value agrees with numerically computed and experimental results found in [36, 38], which gives values ranging from 1.14 to 1.9 J/m^2 for different lattice planes of silicon crystal. Therefore, the adhesive energy, ϖ, is chosen as 2.54 J/m^2 for polysilicon surfaces in this work.

Note that the Hamaker constant considered, thus the above deduced surface energy, are valid for the contact of surfaces made of pure silicon only, meaning not contaminated by a medium. In wafer bonding literature, this range of values was reported from molecular dynamic simulations and was measured experimentally at room temperature in ultra-high vacuum environment for perfectly cleaned surfaces, [39, 40], where adhesion energy can reach 3.6 to 4.8 J/m^2 for some lattice planes [40].

In the presence of a medium, the surface can be contaminated by radicals (e.g. OH-) or oxides (SiO_2) and the adhesive energy will be drastically decreased. The nature of these radicals and oxides depends on the manufacturing process and/or on the room environment. This is briefly described here below, a complete description can be found in [40]. The surfaces will be covered by an oxide terminated by silanol (SI-OH) groups, which are highly hydrophilic. As a result, at room temperature, the bonding is mainly due to OH-groups and the resulting adhesive energy for hydrophilic silicon surfaces have been measured in dry environment to be of the order of 160-320 mJ/m^2, [40] (without considering capillary forces). Upon thermal treatment, hydrophilic surfaces evaporate water molecules and the resulting siloxane (Si-O-Si) bonds result in an adhesion energy of about $\varpi = 2.5$ J/m^2 [40]. For completeness, if the oxide is removed by fluoride-base etching, e.g., the resulting hydrophobic surfaces bond at room temperature due to the Si-H groups exhibiting an adhesive energy of the order of 40-60 mJ/m^2 and bond at high temperature as pure silicon with an adhesive energy $\varpi > 2$ J/m^2 [40]. However, hydrophobic surfaces can, in some cases, be contaminated by hydrocarbons that may be present in air. In clean-room bonding processes, the contaminants may become nucleation sites at which interface bubbles can form [40].

Therefore the choice $\varpi = 2.54$ J/m^2 is a particular case of high-vacuum or high temperature bonding, while in the air a Hamaker constant of 1.865 10^{-19} J was measured [41, page 50], leading to an adhesion energy due to the van der Waals effect in the range of $\varpi = 0.167$ J/m^2.

In this paper we will consider these two last cases, remembering that, as capillary forces are neglected, the later case will be valid below 30% of relative humidity [4].

In the definition of the Dugdale assumption, the critical value of separation z_0 satisfies $\varpi = \sigma_0 z_0$, with σ_0 the maximum adhesive traction resulting from the inter-atomic potential derivation (e.g. Lennard-Jones). Therefore, for usual potential descriptions [32, 33], it can be deduced that $z_0 \approx 0.97 \times 2^{1/6} \times r_0$, and $z_0 \approx 0.97 \times 2^{1/6} \times 2.09$ Å ≈ 2.28 Å for silicon to silicon contact.

B. Statistical Characters of Surface Topography

In the Greenwood-Williamson (GW) model the three important parameters are; the assumed constant radius of the spherical asperities R, the standard deviation of the asperity heights σ_s (assumed to be a Gaussian distribution), and the

surface density of asperities N. In the study of Poon and Bhushan [42], the standard deviation of the asperity heights is referred to as the root-mean-square (RMS) roughness, R_q, when the reference plane is the same as the mean plane. In the following model the standard deviation of asperity heights, σ_s, considers only the tip of asperity heights according to GW model, and not the whole profile of the asperity as for evaluating R_q. According to the research of McCool [43], these three parameters can be extracted from the three spectral moments of the surface topography $z(x,y)$. The three spectral moments include the variance of heights m_0, slope m_2 and curvature m_4, which are expressed as [44]

$$m_0 = \left\langle z^2 \right\rangle, \quad m_2 = \left\langle \frac{dz}{dx} \right\rangle, \quad m_4 = \left\langle \frac{d^2 z}{dx^2} \right\rangle \tag{14}$$

where x is an arbitrary direction and brackets < > represent a statistical average. As m_0 is the mean square surface height, the RMS roughness is $R_q = (m_0)^{1/2}$.

The three statistical surface parameters of the GW model can then be calculated from the following expressions [43]:

$$R = \frac{3\sqrt{\pi}}{8\sqrt{m_4}} \tag{15a}$$

$$N = \frac{1}{6\sqrt{3}\pi}\frac{m_4}{m_2} \tag{15b}$$

$$\sigma_s = \sqrt{m_0 - \frac{3.717\times10^{-4}}{N^2 R^2}} \tag{15c}$$

Since the surface topography $z(x,y)$ can be obtained directly from atomic force microscopy (AFM) measurements, all these statistical surface parameters can be derived from AFM measurements. Evidently, apparatus resolutions and sample lengths will affect these surface parameters, which, in turn, will affect the application of the rough surface contact theory [45]. In order to predict the in-use stiction of MEMS devices, a sample of length, L, comparable to the characteristic dimension of MEMS structures, is suggested during the measurements of the statistical characters of the surface.

For the polysilicon contact problem considered in this paper, although a rather important number of typical surface roughness measurements are available in the literature, usually only the RMS (R_q) of the surfaces is reported. For example, a typical polysilicon surface RMS roughness between 2 and 5 nm was obtained by Delrio et al. [46], while Legtenberg [47] measured an RMS roughness between 1 and 3 nm, depending on polysilicon and sacrificial (PECVD) silicon oxide thicknesses.

However, only an amplitude description of the surface is insufficient for modeling purposes. For this reason, topography measurements using AFM need to be performed on micro-surfaces fabricated by commercial micro-foundries. Based on the AFM measurements, the statistical characters of two interacting surfaces can be obtained from Eqs. (15). Therefore, the statistical characters of the equivalent rough surface can be deduced from the properties of the two surfaces; σ_s, R and K can be directly obtained from the definitions of section II A, and Eqs. (15) are then used in order to extract the missing property N of the equivalent rough surface.

Such analyses were achieved in [48] for a polished silicon film of roughness R_q = 1 nm. This sample will be referred to as sample A in the following. Sample B was analyzed in [49] and consists in an array of polysilicon cantilevers, of different lengths, interacting with landing polysilicon pads. The array was fabricated by repeated deposition, lithographic definition, annealing and etching of polysilicon and sacrificial silicon oxide layers. After dissolution of the sacrificial oxide layers, critical-point drying was performed. A roughness of R_q = 2.67 nm was found for the equivalent rough surface of the two interacting polysilicon surfaces. The original purpose of this cantilever beams array [49, 50] is to study the stiction phenomenon between polysilicon surfaces. In [35], micromachined flaps were fabricated using a three-layer polysilicon surface micromachining process; silicon wafers, deposited silicon nitride and alternating layers of low pressure chemical vapor deposition of sacrificial (silicon dioxide) and structural (polysilicon) layers. This process was followed by a released procedure; etching of the silicon oxide layer using 49% HF, DI water and isopropyl alcohol (IPA) rinses and finally drying. For sample C, the interaction of 2 rough surfaces corresponding to the bottom of the first structural polysilicon layers, having a roughness of R_q = 2.455 nm, is considered. The statistical characters of the equivalent rough surfaces of the samples A-C are reported in Tab. I.

The validity of the elastic contact model, based on a Gaussian distribution assumption, can be ascertained by considering the plastic parameter proposed by GW [19, 20]

$$\psi = \frac{E'}{H}\sqrt{\frac{\sigma_s}{R}} \tag{16}$$

where $E' = E/2/(1-\nu^2)$ and where H is the hardness [49].

When $\psi < 0.6$ the deformations remain elastic and when $\psi > 1$, the deformations are predominantly plastic. Using the typical values for polysilicon: H = 11 GPa, E = 163 GPa and Poisson's ratio = 0.22 [49, 50], the plastic parameters of the three equivalent rough surfaces are evaluated and presented in Tab. I. The maximum plastic parameter is 0.77, corresponding to an amount of plasticity that can be neglected during contact [49]. In cases of polysilicon with higher roughness, or other materials as gold, elasto-plastic behavior could happen, modifying the surface topography [51].

For completeness, the jump-in induced yield criterion developed in [16] is also verified. Although this criterion was developed for the interaction of two spheres of identical tip radii and with a FCC crystal pattern, it gives an estimation of the risk of plasticity in our case. In order to evaluate this criterion the Tabor number [7] is computed first

$$\mu_T = \sqrt[3]{\frac{R\varpi^2}{E'^2\left(2^{1/6} r_0\right)^3}} = \sqrt[3]{\frac{\widetilde{R}}{\widetilde{E}^2}} \tag{17}$$

In Eq. (17), two new dimensionless parameters $\widetilde{R}$ and $\widetilde{E}$ are defined, [16], as

$$\widetilde{E} = \frac{E' 2^{1/6} r_0}{\varpi} \tag{18}$$

$$\widetilde{R} = \frac{R}{2^{1/6} r_0} \tag{19}$$

Using these formulas, the dimensionless Young modulus $\widetilde{E}$ is found to be equal to 7.9 for all the samples with ϖ = 2.54 J/m^2, and equal to 120 for all the samples with ϖ = 0.167 J/m^2. The Tabor parameters (17) and the dimensionless radii (19) are reported in Tab. I. Following [16] for two identical asperities, if the dimensionless Young modulus $\widetilde{E}$ is much larger than 4, or if the dimensionless radius $\widetilde{R}$ is larger than 600, jump-in will not induce plasticity, validating our elasticity assumption.

TABLE I
STATISTICAL CHARACTERS AND THE MECHANICAL PROPERTIES OF THE SI EQUIVALENT ROUGH SURFACE

Equivalent rough surface	R_q nm	σ_s nm	R μm	N μm^{-2}	Ψ	μ_T	$\widetilde{R}$
A. Polished Polysilicon [48]	1.40	1.23	1.70	17	0.21	4.87	7246
B. Deposited Polysilicon [49]	2.67	2.50	0.26	80.1	0.77	2.61	1108
C. Deposited Polysilicon [35]	3.47	3.37	0.62	37.8	0.58	3.48	2643

C. Adhesive Contact Force between Polysilicon-Polysilicon Rough Surfaces

In order to predict the adhesive-contact vs. distance curve of polysilicon-to-polysilicon interactions, the parameters of the equivalent rough surfaces reported in Tab. I are substituted into Eq. (3) to evaluate the Maugis transition parameters λ. For the adhesive parameters ϖ =2.54 J/m^2 and z_0 = 2.28 Å, accordingly to the discussion of the previous section, values of λ=5.6536, λ=3.0234 and λ= 4.0393 can be obtained for the samples A, B and C respectively, while standard deviations of asperity heights σ_s=1.23 nm, σ_s=2.50 nm and σ_s=3.37 nm have been reported for the samples A, B and C respectively.

Following the argument presented in section II, for each couple of λ, σ_s completed by the asperity radius R and the surface density N reported in Tab. I, the unloading adhesive contact-force, F_{nT}, of the equivalent rough surface can be deduced for any separation distance, d. Indeed, from the dimensionless value of d, integral (12) can be performed numerically in terms of the dimensionless approach (interference) Δ (9), while the dimensionless force F_n (8) of a single asperity evaluated at Δ is obtained by solving the set of Eqs. (4-6). This set of equations holds as Kim et al. [31] extended solution should be considered when λ<0.938 only, which is not the case here.

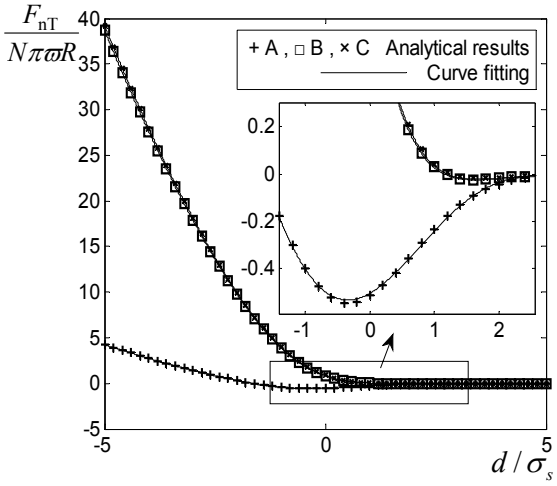

Fig. 5. The normalized adhesive contact force vs. the normalized distance between the rough surfaces for ϖ =2.54 J/m^2: A. λ=5.6536, σ_s=1.23 nm; B. λ=3.0234, σ_s=2.50 nm and C. λ= 4.0393 and σ_s=3.37 nm.

The resulting normalized adhesive contact forces vs. the normalized distance are presented in Fig. 5. From this figure it can be seen that the adhesive contact force vs. the normalized distance curves for samples B and C almost coincide. This is due to the counter-balanced effects of λ (larger for sample C) and σ_s (larger for sample C) when curves are normalized. Sample A, which was obtained after surface polishing, exhibits a different normalized curve.

Generating the curves illustrated in Fig. 5 is time consuming. To overcome this, the multiscale model will use a fitting of the computed curves in order to use finite-element simulations in an efficient way. For example, sample A is fitted using a polynomial approximation of coefficients p_i, following

$$\frac{F_{nT}}{N\pi\varpi R} = \sum_{i=1}^{10} p_i \times (d/\sigma_s)^{10-i} \tag{20}$$

The polynomial coefficients are listed in Tab. II, and a good agreement between the analytical results and the curve fitting results can be observed in Fig. 5.

TABLE II
POLYNOMIAL CURVE FITTING COEFFICIENTS FOR THE NORMALIZED ADHESIVE CONTACT FORCE VS. THE NORMALIZED DISTANCE BETWEEN THE ROUGH SURFACES OF SAMPLE A, WITH ϖ =2.54 J/M^2

i	1	2	3	4	5
p_i	3.283e-006	-6.351e-006	-0.0002217	0.0003907	0.005789
i	6	7	8	9	10
p_i	-0.00932	-0.08042	0.1926	0.1545	-0.5047

These results are related to a work of adhesion ϖ = 2.54 J/m^2, which can be obtained in ultra-high vacuum environment for perfectly cleaned surfaces only [39, 40]. In order to study the environmental effects, the same computations are performed with a Hamaker constant equal to 1.865 10^{-19} J, which is a measured value for contact between 2 silicon surfaces in air [41], yielding a work of adhesion ϖ = 0.167 J/m^2.

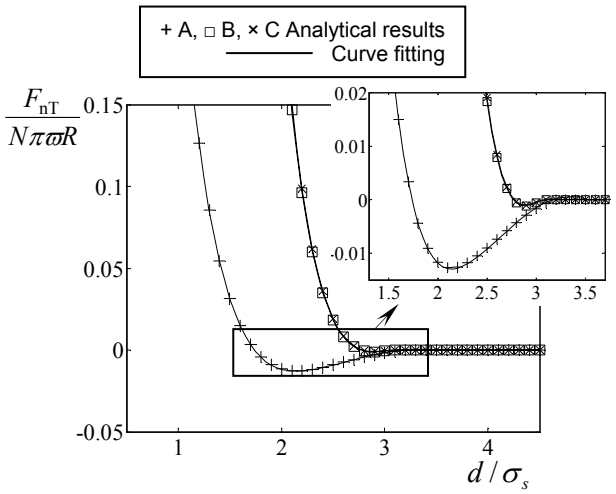

Fig. 6. The normalized adhesive contact force vs. the normalized distance between the rough surfaces for ϖ =0.167 J/m^2: A. λ=0.921, σ_s=1.23 nm; B. λ=0.4925, σ_s=2.50 nm and C. λ= 0.6580 and σ_s=3.37 nm.

Following the same argument, the resulting normalized adhesive contact force vs. the normalized distance curves can be computed. These are presented in Fig. 6. For these lower values of adhesion energy, the maximum adhesion forces are lower and always happen for positive interacting distances, even for polished polysilicon (sample A). Let us note that in this case Kim extension [31] should be considered as λ<0.938 for the three samples.

IV. Multi-Scale Finite Element Analysis

A. Problem Description

A typical MEMS problem, which consists of a cantilever suspended above a surface, is considered as an example in this work. Indeed such applications are commonly used to study stiction problems, [25, 26, 49, 50], and will be used to compare our results to data found in literature. Assuming contact between the cantilever and the surface has been established, accidentally or on purpose, the beam is subjected to an unloading process during which the adhesive-contact forces, described in section II, rule the beam-surface interaction. There are three possible equilibrium configurations of the beam corresponding to the end of this unloading process; initial configuration, arc-shaped configuration and S-shaped configuration, Fig. 7. The last two configurations correspond to a stiction state. Clearly, the final configurations depend on the degree of adhesion that is established between the two surfaces in contact. In order to avoid in-use stiction, a stiffer cantilever, which can store enough elastic energy to break the contact, is required.

In this section, a finite element analysis is presented based on the adhesive contact model presented in the previous sections. This finite element analysis can be used to predict the stiction of the cantilever beam and to deduce the structure critical geometrical dimensions avoiding this phenomenon.

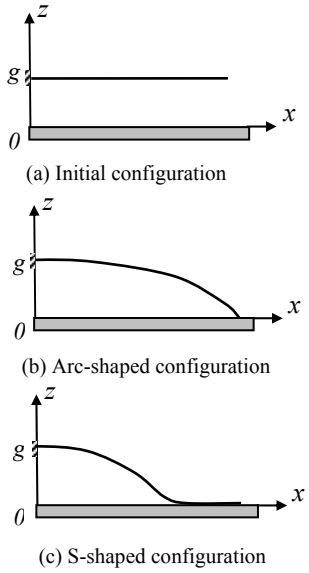

Fig. 7. Three possible equilibrium configurations of the cantilever beam after unloading.

B. Finite Element Model

In this study, a two-dimensional finite element model is used to simulate the deformation of the micro-cantilever beam under the adhesive contact between the beam and the pad. The numerical simulations are performed using a finite element package developed by the authors.

The Timoshenko equations [53] with unknowns w, the transverse displacement, and θ, the angular rotation, for a straight beam directed toward x-axis, are given as

$$\frac{\partial}{\partial x}\left(EI\frac{\partial\theta}{\partial x}\right)-\mu A'\left(\theta+\frac{\partial w}{\partial x}\right)=0 \qquad (21a)$$

$$\frac{\partial}{\partial x}\left(\mu A'\left(\frac{\partial w}{\partial x}+\theta\right)\right)=-f \qquad (21b)$$

where, I is the second moment of inertia, A' is the reduced cross-section area (5/6 of section area for rectangular cross-sections), E and μ are the Young and shear modulus respectively, and f is the force per unit length applied to the beam.

Validity of Timoshenko beam theory is ensured for low slenderness as long as no geometrical or material non-linearities should be considered. For MEMS with rather thin beam thicknesses geometrical non-linearities can be observed due to axial constrains. For this reason, beams are restricted to clamped/free cantilever beams.

The locking-free finite element discretization is based on the interdependent interpolation model presented by Reddy [53]. This model is based on the exact polynomial solution satisfying (21), leading, for one element, to the elementary system

$$\begin{pmatrix} \frac{12EI}{(1+12\Omega)l^3} & \frac{-6EI}{(1+12\Omega)l^2} & \frac{-12EI}{(1+12\Omega)l^3} & \frac{-6EI}{(1+12\Omega)l^2} \\ \frac{-6EI}{(1+12\Omega)l^2} & \frac{4EI(1+3\Omega)}{(1+12\Omega)l} & \frac{6EI}{(1+12\Omega)l^2} & \frac{2EI(1-6\Omega)}{(1+12\Omega)l} \\ \frac{-12EI}{(1+12\Omega)l^3} & \frac{6EI}{(1+12\Omega)l^2} & \frac{12EI}{(1+12\Omega)l^3} & \frac{6EI}{(1+12\Omega)l^2} \\ \frac{-6EI}{(1+12\Omega)l^2} & \frac{2EI(1-6\Omega)}{(1+12\Omega)l} & \frac{6EI}{(1+12\Omega)l^2} & \frac{4EI(1+3\Omega)}{(1+12\Omega)l} \end{pmatrix} \begin{pmatrix} w_1 \\ \theta_1 \\ w_2 \\ \theta_2 \end{pmatrix} = \begin{pmatrix} f_{w1} \\ f_{\theta 1} \\ f_{w2} \\ f_{\theta 2} \end{pmatrix} \quad (22)$$

where $\Omega=\frac{EI}{\mu A' l^2}$ represents the effect of shearing on the beam's deflection, and where w_1, w_2, θ_1, θ_2 are the nodal displacements and rotations of the beam element of length l.

The loading vector is evaluated from a linear distribution of force per unit length: $f=f_0+(f_1-f_0)\,x/l$. Following an integration of shape functions presented in [53], this leads to

$$\begin{pmatrix} f_{w1} \\ f_{\theta 1} \\ f_{w2} \\ f_{\theta 2} \end{pmatrix}_{cst} = \frac{lf_0}{2} \begin{pmatrix} 1 \\ -\frac{l}{6} \\ 1 \\ \frac{l}{6} \end{pmatrix} \quad (23a)$$

$$\begin{pmatrix} f_{w1} \\ f_{\theta 1} \\ f_{w2} \\ f_{\theta 2} \end{pmatrix}_{lin} = \frac{l(f_1-f_0)}{20+240\Omega} \begin{pmatrix} 3+40\Omega \\ -\left(\frac{2}{3}+10\Omega\right)l \\ 7+80\Omega \\ (1+10\Omega)l \end{pmatrix} \quad (23b)$$

for the constant and linear parts of the applied force respectively.

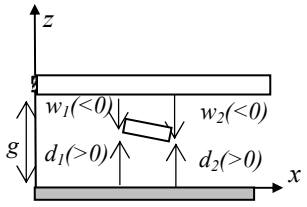

Fig. 8. Schematic of the beam element.

A schematic of the beam element is reported in Fig. 8. It is clear that the nodal distance d_i between the lower face of the beam and the pad can be deduced from the nodal displacement w_i

$$d_i = g + w_i \quad (24)$$

Therefore, the force per unit length f_i at node i can be deduced from the curve fitting of the adhesive contact analysis presented in sections II and III, and Eq. (20) yields

$$f_i = bF_{\mathrm{nT}}(d_i) \quad (25)$$

where b is the beam width. Assuming a linear distribution of force on one beam element, which is a reasonable approximation if the mesh is fine enough, the elementary forces can be evaluated from Eqs. (23).

In order to simulate accurately the variation of the adhesive contact forces under important gradient of contact distances, a much finer finite element mesh size is required at the contact part of the micro cantilever beam. Typically, the beam is discretized into 128 elements with elements at beam's tip having a size ten times smaller than at the built-in end.

Note that Eq. (25) is correct only during the unloading process. In order to simulate the happening of contact an extra force is applied on the top beam surface until the cantilever enters into the contact with the surface. Thereafter, this extra force is removed step by step until reaching zero. At this stage only the adhesive contact forces are acting on the beam. The possible configurations of the beam under the adhesive contact forces can be obtained afterwards. The geometrical effects of the micro cantilever beams such as the initial gap size, the thickness and length, which are critical in order to avoid stiction, can now be studied for different adhesive contact conditions of rough surfaces.

V. Results and Discussion

The adhesive contact between polysilicon cantilever beams and polysilicon surfaces is considered in this section. A typical value of 163 GPa [49, 50] for the elastic modulus of polysilicon is used in the finite element simulations of the beam. Relative parameters of the adhesive contact, which include surface characters and material properties, have been established in Section III.

First, a 4-μm thick and 20-μm wide beam is considered. The initial gap between the beam and the surface is 2 μm, and the surface parameters of cleaned silicon surfaces in an ultra-high vacuum (ϖ =2.54 J/m^2) correspond to sample A. The beam deflection due to self-weight is neglected. Figs. 9(a-c) illustrate the final results obtained for beam lengths of 50, 90 and 120 μm successively.

Depending on its length, the beam is either, not subject to stiction during the unloading process (Fig. 9(a)), or subject to stiction with an arc-shaped configuration or an S-shaped configuration (Figs. 9(b-c)). From the simulations it can be concluded that; (1) when the length of the beam is larger than a certain value l_1, stiction with an arc-shaped configuration will be obtained, (2) increasing the length of the beam up to a certain value l_2 will lead to stiction with an S-shaped configuration, (3) for beam lengths $l_1 < l < l_2$ [26, 27], the final configuration may shift between the arc-shaped and the S-shaped configurations, depending on the initial contact configurations.

Both arc-shaped and S-shaped configurations correspond to stiction. Therefore, as $l_1 < l_2$, the beam length l_1 is set to be the critical design length. For the same contact conditions the design limitations avoiding in-use stiction are now calculated in terms of the beam's geometrical dimensions. Fig. 10 presents

the design limitations in terms of thickness vs. length of the beam for initial gap sizes equal to 1, 2 and 3μm successively.

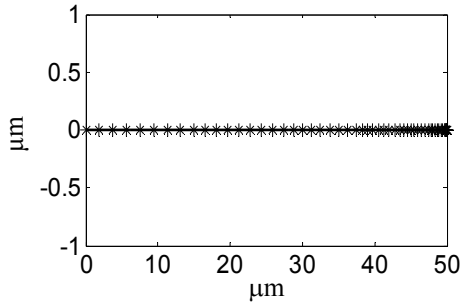

(a) Beam length = 50 μm

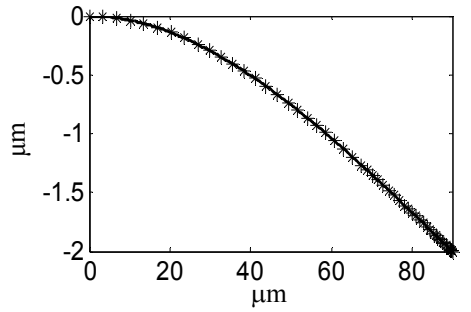

(b) Beam length = 90 μm

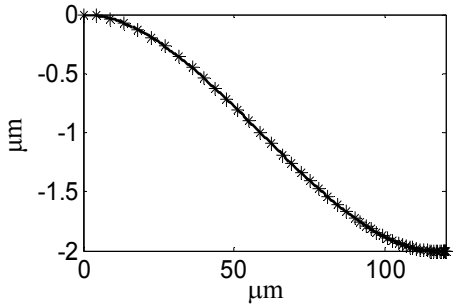

(c) Beam length = 120 μm

Fig. 9. Final configurations of the micro-cantilever beams for different lengths, for ϖ =2.54 J/m^2.

The design range of the ratio thickness/length, avoiding stiction, is defined as the area above the design limitations for given initial gap sizes. From Fig. 10, it can be seen that, at constant thickness, a smaller initial gap size requires a shorter beam length in order to avoid in-use stiction.

Considering the initial gap size of 2 μm, the effect of surface roughness on stiction can also be studied by considering the different surface samples A-C, the characteristics of which are reported in Tab I. Fig. 11 illustrates the limitations in terms of the thickness vs. length of the beam obtained from the finite element simulations for the different surface states. As expected, the polished silicon surface is more prone to stiction as its roughness is lower. Although dimensionless adhesive contact curves for surfaces B and C are similar, Fig. 5, numerical results exhibit different safe design parameters, Fig. 11. Indeed, although the sample C has a higher roughness than sample B, the combined effect of asperity tip radius and asperity density per unit area leads to a higher maximum adhesive force for sample C, thus more subject to stiction.

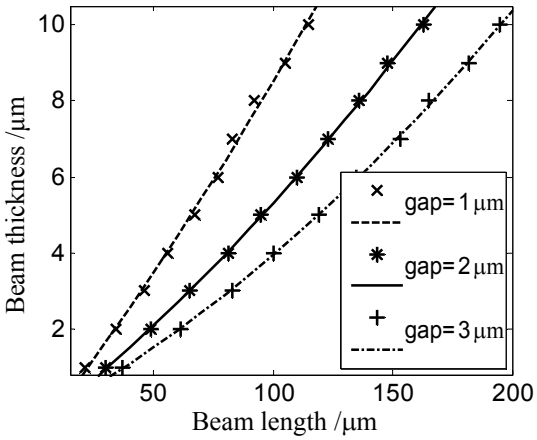

Fig. 10. The design limitations to avoid stiction of the micro cantilever beams with different initial gap sizes (the marks correspond to finite element results and the curves to quadratic fitting results) for ϖ =2.54 J/m^2.

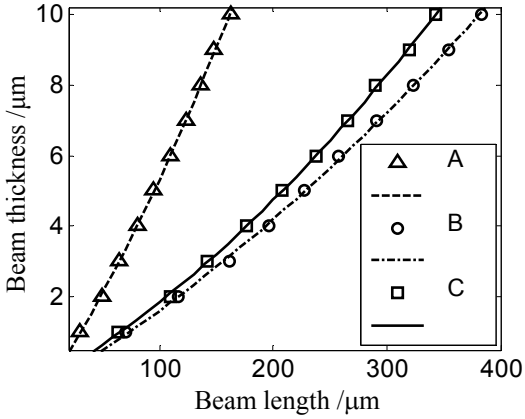

Fig. 11. The design limitations to avoid stiction for the different surface samples (the marks correspond to finite element results and the curves to quadratic fitting results) for ϖ =2.54 J/m^2.

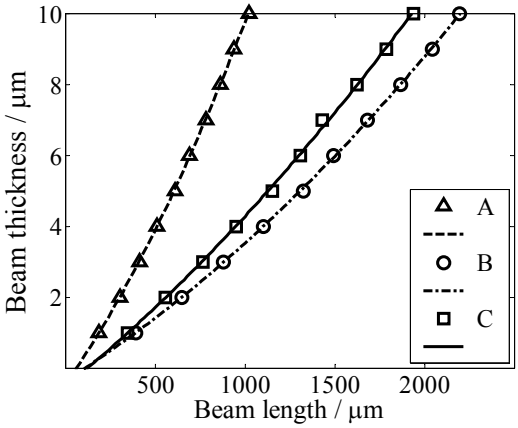

Fig. 12. The design limitations to avoid stiction for the different surface samples (the marks correspond to finite element results and the curves to quadratic fitting results) for ϖ =0.167 J/m^2.

Similar results can be obtained readily for ϖ =0.167 J/m^2, by considering the unloading force-distance curves of Fig. 6 instead of Fig. 5. Fig. 12 illustrates the new limitations in terms

of the thickness vs. length of the beam obtained from the finite element simulations for the different surface states, and shows similar behaviors as when ϖ =2.54 J/m^2 , Fig. 11. The only difference is the critical lengths of the beam, which, as expected, are approx ten times higher with the low adhesion energy.

From Fig. 11 and Fig. 12, it can be concluded that the roughness and asperities tip radius of the surfaces in contact have an important nonlinear effect on the stiction in MEMS devices. For the MEMS with polished surfaces in contact, a thick and short beam is required to avoid stiction.

VI. Results Comparison

In order to compare our model and our results with models and experimental measurements from the literature, the apparent adhesion energy resulting from the interacting rough surfaces is extracted from the numerical results presented in section V.

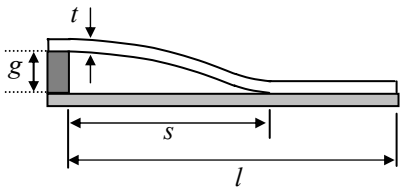

(a) S - shaped cantilever beam

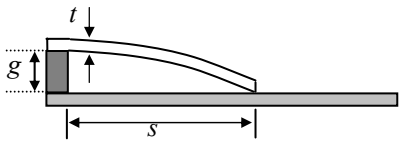

(b) Arc - shaped cantilever beam

Fig. 13. Schematics of adhered micro-cantilevers.

In [26], it is shown that the apparent adhesion energy Γ can be deduced from studying an array of cantilevers of different lengths. Indeed from the sticking beams of the array, either in an S-shaped configuration, Fig. 13(a), or in an arc-shaped configuration at critical length (shortest length), Fig 13(b), the apparent adhesion energy, Γ, can be evaluated in terms of the un-adhered length, *s*, with

$$\Gamma = \frac{3}{2} E \frac{g^2 t^3}{s^4} \tag{26}$$

and

$$\Gamma = \frac{3}{8} E \frac{g^2 t^3}{s^4} \tag{27}$$

respectively.

In section V, critical lengths leading to arc-shaped configurations have been evaluated numerically with our model for different beam thicknesses and for the 3 different surface samples A-C. Using relation (27), the apparent adhesion energy, Γ, can be directly computed from Fig. 11. The results are reported on Fig. 14.

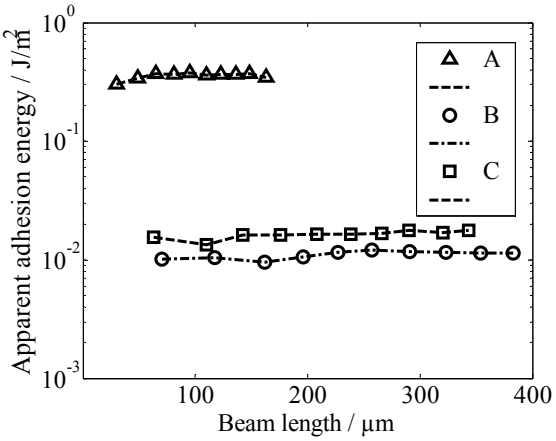

Fig. 14. Apparent surface energy Γ deduced from the critical arc-shaped configurations for ϖ =2.54 J/m^2.

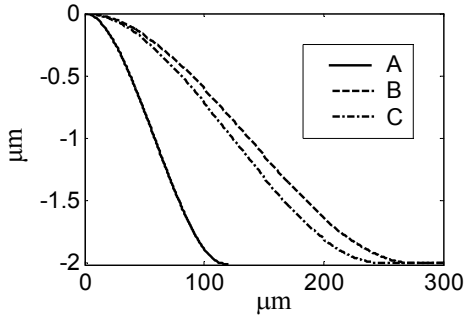

Fig. 15. Final configurations of the micro-cantilevers for different beam lengths. *s* = 115, 280, 250 μm for sample A, B and C respectively, and for ϖ =2.54 J/m^2.

It can be seen that, with the exception of the shortest beam, which does not obey the Euler-Bernoulli assumption used in (27), the apparent surface energies evaluated are constant for a given surface sample. Due to the important effect of surface properties which include the surface roughness, but also the asperities tip radius and the asperities density, the apparent adhesion energies of sample A, B and C differ from each other. Although it is admitted that Γ should decrease with an increase of the roughness, the sample C, which has a higher roughness than sample B, yields higher apparent adhesion energy than B due to the larger asperities tip radius of its surface.

TABLE III
Apparent Adhesion Energy for the Three Rough Surfaces

	A	B	C
R_q (nm)	1.4	2.67	3.47
Γ (mJ/m^2) for ϖ =2.54 J/m^2	357	10.2	16.0
Γ (mJ/m^2) for ϖ =0.167 J/m^2	0.22	0.0105	0.0184

In order to confirm results of Fig. 14, data for S-shaped sticking cantilevers are also analyzed. Resulting sticking configurations of beams for an initial gap size of 2 μm, and for a beam thickness of 4 μm, are illustrated, Fig. 15, for the 3

different surface samples. The respective apparent adhesion energies (26) are reported in Table III.

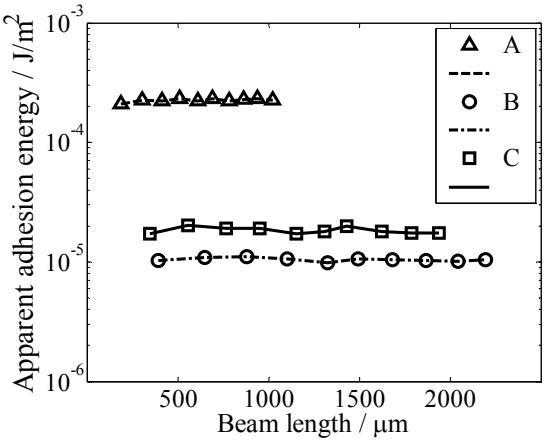

Fig. 16. Apparent surface energy Γ deduced from the critical arc-shaped configurations for ϖ =0.167 J/m^2.

These previous results are related to a work of adhesion ϖ = 2.54 J/m^2. In order to study the environmental effect, the same computations are performed for contaminated surfaces in air with low relative humidity (ϖ = 0.167 J/m^2). In order to avoid the effect of capillary forces, the relative humidity should be lower than 30%. From critical lengths from Fig. 12, the apparent adhesion energies Γ can be directly computed from Eq. (27) and are shown in Fig. 16. It can be seen that for each surface sample this energy is rather constant but much lower than for the case of pure silicon contact. The average values are reported in Table III.

In [4], the van der Waals energy was integrated using a Gaussian asperity height distribution. A Hamaker constant of 2 10^{-19} J was assumed in order to compute the resulting apparent adhesion energy in the absence of capillary forces. This curve is given in Fig. 17 in terms of the RMS-roughness characterizing the height distribution. Numerical results obtained with the presented model seem to correlate with the curve, at least when using the measured Hamaker constant, [41]. Although the analytical prediction is monotonically decreasing with the RMS-roughness, as more surface properties (density, tip radius, etc) are accounted for in the developed model, this trend is not reproduced.

Surface properties of sample A were considered to study the effect of the sub-lubrication on the adhesion model in [48]. In this model the lubricant is too thin to produce meniscus, but leads to adhesion forces. Adhesion forces are modeled using a Lennard-Jones attractive potential coupled with a GW asperity model extended to elasto-plasticity [54]. This model allows extracting force-distance curves, and could theoretically be used in a micro-macro model (as presented here). The presence of a lubricant film in [48] prevents comparison of results as dry contact is assumed herein, lowering the adhesion forces.

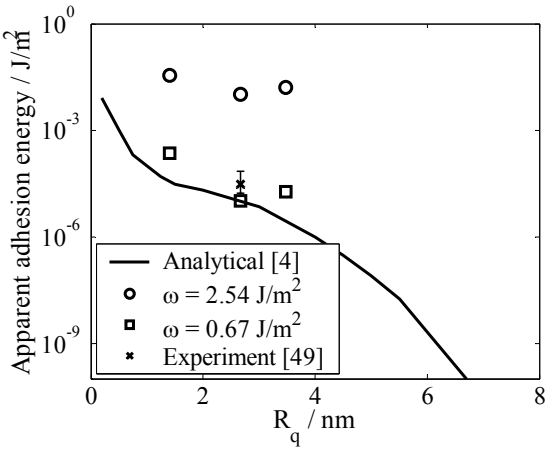

Fig. 17. Comparison of the apparent surface energy Γ with literature.

In [27, 49], experiments were conducted on cantilevers with hydrophilic surfaces obtained from deposited polysilicon, corresponding to sample B. Although the purpose of these papers was to study the effect of capillary forces, experiments were also conducted in dry-nitrogen environment to annihilate the capillary effect. For an RMS-roughness of 2.67 nm, the measured apparent adhesion energies were reported between 0.017 and 0.068 mJ/m^2. This interval is also shown in Fig. 17. In the works [27,49], the van der Waals contribution to the apparent adhesion energy (main interest of the papers is to account for the capillary forces) is obtained by combining a DMT model [6] with a Gaussian height distribution. However, these numerical results exhibit lower apparent adhesion energies by a few orders of magnitude than the experiments, unless the Gaussian distribution is cut-off [27, 49]. In contrast, the presented model, based on the Maugis transition solution and on Kim extension, seems to corroborate the experimental results, although it can be seen that the result is still slightly below the experiments. This can be explained by the fact that the capillary forces were neglected and that they might still be present in the experiments.

Surface sample C was considered in [35] to predict the adhesion energy resulting from a meniscus and results cannot be compared with our predictions as dry environment was assumed.

The main advantage of the presented model is its ability to account for a wide variety of micro-scale parameters (surface topography, surface cleanness, etc), while still allowing complete modeling of MEMS structures using a finite element method. If asperities remain elastic the use of the Maugis solution combined with Kim extension ensures a wide range of validity in terms of surface properties. However, the current limitation of the model is the assumption of dry environment and the effect of capillary forces will have to be accounted for in the near future.

VII. Conclusions

A micro-macro multi-scale approach was developed in order to predict possible in-use stiction of MEMS devices resulting from the van der Waals interaction forces.

At the lower scale the unloading adhesive contact-distance curves of two interacting rough surfaces were established from a combination of the Greenwood-Williamson asperity model and the Maugis transition theory. The computed unloading adhesive contact-distance curves are dependent on the material and surface properties as well as on the rough surfaces topography parameters. This model was integrated at the higher scale as an adhesive-contact force at the beam-substrate interface, using a finite element analysis.

By way of illustration the parameters required to define the micro adhesive contact curves were identified for polysilicon-to-polysilicon interactions. These parameters were either evaluated from theoretical models, surface energy measurements or from AFM measurements.

Prediction of stiction of cantilever beams in terms of thickness, beam-to-surface gap and length, for polysilicon-to-polysilicon interacting surfaces was then achieved. Critical thickness curves in terms of beam length could then be obtained for different initial gaps. The effect of the surface topography on these design parameters was also studied by considering different surface states.

From the critical lengths of the beam the apparent surface energies could be computed and were shown to be in good agreement with experimental data from the literature, when contaminated polysilicon surfaces in dry air were considered.

In the current work the multi-scale approach was developed to predict stiction in MEMS devices in dry working environments. The main advantage of this approach is its ability to account for different surface and material properties, which can be measured for a given structure. Also, a simple linear cantilever beam was studied, but the approach can be generalized to other kinds of MEMS devices.

References

[1] A. Hariri, J. W. Zu and R. Ben Mrad, "Modeling of dry stiction in micro electro-mechanical systems (MEMS)," *IEEE J. Micromech. Microeng*, vol. 16, pp. 1195–1206, 2006.

[2] W. Robert Ashurst, C. Yau, C. Carraro, R. Maboudian, and M. T. Dugger, "Dichlorodimethylsilane as an Anti-Stiction Monolayer for MEMS: A Comparison to the Octadecyltrichlosilane Self-Assembled Monolayer," *IEEE J. Micromech. Systems*, vol. 10, pp. 41-49, 2001.

[3] W. M. van Spengen, R. Puers and I. De Wolf, "A physical model to predict stiction in MEMS," *J. Micromech. Microeng.*, vol. 12, pp. 702-713, 2002.

[4] W. M. van Spengen,, R. Puers and I. De Wolf, "On the physics of stiction and its impact on the reliability of microstructures," *J. Adhesion Sci. Technol*., vol. 17, no. 4, pp. 563–582, 2003.

[5] K. L. Johnson, K. Kendall and A. D. Roberts, "Surface Energy and the Contact of Elastic Solids," *Proc. R. Soc. Lond. A*, vol. 324, pp. 301-313, 1971.

[6] B. V. Derjaguin, V. M. Muller and Y. P. Toporov, "Effect of contact deformation on the adhesion of elastic solids," *J. Colloid Interface Sci.* vol. 53, pp. 314–26, 1975.

[7] D. Tabor, "Surface forces and surface interactions," *J. Colloid Interface Sci.*, vol. 58, pp. 2-13, 1977.

[8] D. Maugis, "Adhesion of Spheres: The JKR-DMT Transition Using a Dugdale Model," *J. Colloid and Interface Sci.*, vol. 150, pp. 243-269, 1992.

[9] L. Kogut and I. Etsion, "Adhesion in elastic–plastic spherical microcontact," *J. Colloid and Interface Sci.*, vol.261, pp. 372–378, 2003.

[10] Y. Kadin, Y. Kligerman, and I. Etsion, "Loading–unloading of an elastic–plastic adhesive spherical microcontact," *J. of Colloid and Interface Sci.*, vol. 321, pp. 242–250, 2008.

[11] L. Johnson and J. A. Greenwood, "An Adhesion Map for the Contact of Elastic Spheres," *J. Colloid Interface Sci.*, vol. 192, pp. 326-333, 1997.

[12] P. Attard and J. L. Parker, "Deformation and adhesion of elastic bodies in contact," *Phys. Rev. A*, vol. 46, pp. 7959-7971, 1992.

[13] V. M. Muller, V. S. Yushchenko, and B. V. Derjaguin, "On the influence of molecular forces on the deformation of an elastic sphere and its sticking to a rigid plane," *Progress in Surface Sci.*, vol. 45, pp. 157-167, 1994.

[14] J. A. Greenwood, "Adhesion of elastic spheres," *Proc. R. Soc. London A*, vol. 453, pp. 1277-1297 ,1997.

[15] R. Gissi, and P. Decuzzi, "The effect of shape and size in micro-/nanodimples adhesion," *ASME J. Appl. Phys.*, vol. 98, Paper 014310, 2005.

[16] Y. Kadin, Y. Kligerman, and I. Etsion, "Jump-in induced plastic yield onset of approaching microcontacts in the presence of adhesion," *ASME J. Appl. Phys.*, vol. 103, Paper 013513, 2008.

[17] Y. Kadin, Y. Kligerman, and I. Etsion, "Cyclic loading of an elastic-plastic adhesive spherical microcontact," *ASME J. Appl. Phys.*, vol. 104, Paper 073522, 2008.

[18] Y. Du, L. Chen, N. E. McGruer, G. G. Adams, I. Etsion, "A finite element model of loading and unloading of an asperity contact with adhesion and plasticity," *J. Colloid Interface Sci.*, vol. 312, pp. 522-528, 2007.

[19] J. A. Greenwood and J. B. P. Williamson, "Contact of nominally flat surfaces," *Proc. R. Soc. Lond. A*, vol. 295, pp. 300–19, 1966.

[20] J. A. Greenwood and J. H. Tripp, "The contact of two nominally flat rough surfaces," *Proc. Instn Mech. Eng.*, vol. 185, pp. 625–33, 1971.

[21] S. Patra, S.M. Ali and P. Sahoo, "Elastic–plastic adhesive contact of rough surfaces with asymmetric distribution of asperity heights," *Wear*, vol. 265, pp. 554–559, 2008.

[22] L. Wu, V. Rochus, L. Noels, and J. C. Golinval, "Influence of adhesive rough surface contact on microswitches," *ASME J. Appl. Phys.*, vol. 106, Paper 113502, 2009.

[23] B. B. Mandelbrot, *The Fractal Geometry of Nature*. Freeman, New York, 1983.

[24] A. Majumdar and B. Bhushan, "Fractal model of elastic–plastic contact between rough surfaces," *ASME J. Tribol.*, vol. 113, pp. 1–11, 1991.

[25] N. Tas, T. Sonnenberg, H. Jansen, R. Legtenberg and M. Elwenspoek, "Stiction in surface micromachining," *IEEE J. Micromech. Microeng*., vol. 6, pp. 385–397, 1996.

[26] M. P. de Boer, T. A. Michalske, "Accurate method for determining adhesion of cantilever beams," *ASME J. of Appl. Phys.*, vol. 86, no. 2, pp. 817-827, 1999.

[27] M. P. de Boer, J. A. Knapp, T. M. Mayer and T. A. Michalske, "The role of interfacial properties on MEMS performance and reliability," in *Proc. SPIE/EOS Conference on Microsystems Metrology and Inspection*, Munich, June 15, 1999.

[28] L. L. Mercado, S.-M. Koo, T.-Y. Tom Lee, L. Liu, "A mechanical approach to overcome RF MEMS switch stiction problem," in *Proc. 53rd Electronic Components and Technology Conference*, 2003, pp. 377- 384.

[29] R. Ardito, A. Corigliano and A. Frangi, "Finite element modelling of adhesion phenomena in MEMS," in *Proc. 11Th Int. Conf. on Thermal, Mechanical and Multiphysics Simulation in MEMS, EuroSimE*, 2010, Bordeau, France, ISBN: 978-1-4244-7024-2.

[30] M. O'Callaghan and M. A. Cameron, "Static contact under load between nominally flat surfaces in which deformation is purely elastic," *Wear*, vol. 36, pp. 79–97, 1976.

[31] K. S. Kim, R. M. McMeeking and K. L. J. Johnson, "Adhesion, Slip, Cohesive Zones and Energy Fluxes for Elastic Spheres in Contact," *Mech. Phys. Solids*, vol. 46 pp. 243–66, 1998.

[32] R. J. Stokes and D. F. Evans, *Fundamentals of Interfacial Engineering*, Wiley–VCH, New York, 1997.

[33] N. Yu, A. A. Polycarpou, "Adhesive contact based on the Lennard–Jones potential: a correction to the value of the equilibrium distance as used in the potential," *J. of Colloid and Interface Sci.*, vol. 278, pp. 428–435, 2004.

[34] F. Cacchione, "Mechanical characterization and simulation of fracture processes in Polysilicon Micro Electro Mechanical Systems (MEMS)," Ph.D. dissertation, Dipartimento di Ingegneria Srutturale, Politechnico di Milano, 2007.

[35] X. Xue, L. M. Phinney and A. A. Polycarpou, "Asymmetric surface roughness measurements and meniscus modeling of polysilicon surface micromachined flaps," *Microsyst. Technol*., vol. 14, pp. 17–29, 2007.

[36] K. C. Fang and C. I. Weng, "An investigation into the melting of silicon nanoclusters using molecular dynamics simulations," *Nanotechnol.*, vol. 16, pp 250–256, 2005.

[37] J. J. Gilman, "Direct Measurements of the Surface Energies of Crystals," *ASME J. Appl. Phys.*, vol 31, no. 12, pp. 2208-2218, 1960.

[38] C. Messmer and J. C. Bilello, "The surface energy of Si, GaAs, and GaP", *ASME J. Appl. Phys.*, vol. 52, no. 7, pp. 4623-4629, 1981.

[39] U. Gösele, Y. Bluhm, G. Kästner, P. Kopperschmidt, G. Kräuter, R. Scholz, L.-J. Huang, Y.-L. Chao, and T. H. Lee, "Fundamental issues in wafer bonding," *J. Vac. Sci. Technol.*, vol. A 17, no. 4, pp. 1145-1152, 1999.

[40] A. Plößl, G. Kräuter, "Wafer direct bonding: tailoring adhesion between brittle materials," *Mat. Sci. and Engineer*, vol. R25, pp 1-88, 1999.

[41] B. Cappela and G. Dietler, "Force-distance curves by atomic force microscopy," *Surf. Sci. Reports*, vol 34, pp. 1-104, 1999.

[42] C. Y. Poon and B. Bhushan, "Comparison of surface roughness measurements by stylus profile AFM and non-contact optical profiler," *Wear*, vol. 190, pp. 76–88, 1995

[43] J. I. McCool, "Predicting Microfracture in Ceramics Via a Microcontact Model," *ASME J. Tribol.*, vol. 108, pp. 380–386, 1986.

[44] R. W. Carpick, E. E. Flater, J. R. VanLangendon and M. P. de Boer, "Friction in MEMS: from single to multiple asperity contact," in *Proc. Int. Congress and Exposition on Experimental and Applied Mechanics*, 2002, pp. 282–287.

[45] L. Kogut and R. L. Jackson, "A Comparison of Contact Modeling Utilizing Statistical and Fractal Approaches," *J. Tribol.*, vol.128, pp. 213-217, 2006.

[46] F. W. Delrio, M. P. de Boer, J. A. Knapp, E. D. Reedt Jr, P. J. Clews and M. L. Dunn, "The role of van der Waals forces in adhesion of micromachined surfaces," *Nature Materials,* vol. 4, pp. 629-634, 2005.

[47] R. Legtenberg, "Electrostatic actuators fabricated by surface micromachining technique,s" Ph.D. dissertation, University of Twente, 1996.

[48] A. Y. Suh and A. A. Polycarpou, "Adhesion and pull-off forces for polysilicon MEMS surfaces using the sub-boundary lubrication model," *J. of Tribology*, vol. 125, pp. 193-199, 2003.

[49] M.P. de Boer, "Capillary adhesion between elastically hard rough surfaces," *Experim. Mech.,* vol. 47, pp. 171–183, 2007.

[50] F. W. Del Rio, M. L. Dunnb and M. P. de Boer, "Capillary adhesion model for contacting micromachined surfaces," *Scripta Materialia*, vol. 59 pp. 916–920, 2008.

[51] O. Rezvanian, M. A. Zikry, C. Brown and J. Krim, "Surface roughness, asperity contacxt and gold RF MEMS switch behavior," *J. Micromech. Microeng.*, vol. 17, pp. 2006-2015, 2007.

[52] J. H. Kim, D. J. Srolovitz, P.-R. Cha and J.-K. Yoon, "Capillarity and electromigration effects on asperity contact evolution in microelectromechanical systems switches," *ASME J. Appl. Phys*., vol. 100, Paper 054502, 2006.

[53] J.N. Reddy, "On locking-free shear deformable beam finite elements," *Comp. Meth. in Appl. Mech. and Engin.*, vol. 149, pp 113-132, 1997.

[54] A. Tayebi and A. Polycarpou, "Adhesion and contact modeling and experiments in microelectromechanical systems including roughness effects," *Microsyst. Technol.*, vol. 12, pp. 854-869, 2006.